Korean Journal of Remote Sensing, Vol.27, No.3, 2011, pp.213~223

Retrieval of Spherical Ocean Wave Parameters Using RADARSAT-2 SAR Sensor Observed at Chukk, Micronesia

Sudhir Kumar Chaturvedi *, **, Chan-Su Yang ** †, Jung-Hwan Song, Kazuo Ouchi*** and P. Shanmugam***

*Department of Ocean Engineering, Indian Institute of Technology Madras, India

**Korea Ocean Satellite Center, Korea Ocean Research & Development Institute (KORDI), Republic of Korea

***Department of Computer Science, School of Electrical and Computer Engineering, National Defence Academy, Japan

Abstract : The purpose of this study is to estimate the spherical wave parameters that appears in synthetic aperture radar (SAR) image acquired over the coast of Chukk, Micronesia. The retrieval of ocean wave parameters consists of two main stages: the first is to determine the dominant wavelengths by Fast Fourier Transform (FFT) over 16 sub-image areas and the second is to estimate wave slopes and heights using dispersion relationship under various water wave conditions. It is assumed that the spherical waves are linear and progressive. These type of waves have the range and azimuth components traveling in radial directions. The azimuth travelling waves are more affected by the velocity bunching mechanism and it is difficult to estimate the wave parameters for these affected areas in SAR imagery. In order to compensate these effects, the velocity bunching ratio (VBR) based on modulation transfer function (MTF) was compared with the intensity ratio for neighbor area in the radial direction in order to assign the spherical wave properties for azimuthally travelling waves. Dispersion relation provides the good estimates for the wave heights for all the selected sub-image areas in the range of 1m to 2m. VBR based on MTF was found to be 0.78 at wave height of 1.36m, while the intensity-based VBR was 0.69 which corresponds to the height of 1.75m. It can be said that the velocity bunching accounts for azimuthally travelling spherical waves and the difference results from the sea-bottom effects.

Key Words : Spherical waves, Wave parameters, FFT, SAR-ocean imaging, Dispersion relation, Velocity bunching.

1. Introduction

SAR images have provided the potential contribution for measuring the various oceanic phenomena such as estimation of the wavelengths, directions, as well as wave heights under several metrological conditions. Over an ocean, SAR image consists of fine resolution with some rough signatures of oceanographic phenomenon such as waves, currents and internal waves (Vachon and Raney, 1991; Kim, 2009).

The linear system approaches to the SAR imaging mechanism (Alpers, 1983) that provides a basis for a

Received May 13, 2011; Revised May 30, 2011, Revised June 13, 2011; Accepted June 14, 2011.

† Corresponding Author: Chan-Su Yang(yangcs@kordi.re.kr)

procedure to estimate wave height spectra from SAR intensity images. The effectiveness of a linear system approach to SAR wave imaging can be explored through numerical simulation study. These simulations begin with the input ocean spectrum in order to estimate height topography, use of models based on the backscattered signals are as the function of wave height which includes the mapping of intensity levels depending on wind blow over the sea surface.

Retrieval of the ocean wave parameters by SAR depends on sea state. In addition, it also depends on SAR imaging mechanisms such as velocity bunching, tilt and hydrodynamic modulations. The normalized radar cross section (NRCS) for the case of flat sea surface shows negative value of more than −10 dBs (Hasselmann and Hasselmann, 1991; Hasselmann *et al.*, 1996). An analytic expression for the non-linear ocean–to–SAR spectral transform (Krogstad, 1992) is exists which describes the SAR image spectrum as a function of ocean wave fields. It shows the relation for ocean wave spectrum derived from SAR signal spectrum. SAR image spectrum was also obtained through the modulation transfer function (MTF) which produces accurate estimates of slope- and height-variance spectra (Frank and David, 1986).

There are numerous models have been proposed in order to retrieve the wave parameters either in deep or in coastal sea waters using various analytical expressions. Polarimetric analysis (Ouchi and Yang, 2010; Shirato and Ouchi, 2010) is also one way to estimate wave heights with the use of polarimetric ratio of radar cross section for HH- and VV-polarization images for the purpose to estimate the wave slopes by means of pixel based analysis. Co-polarization (HH/VV) image data are less affected by wind and sea states and they shows better response for wave parameter estimation as compared to the cross-polarization (HV/VH) image data (Vachon *et al.*, 1994).

Poor SAR images with low SNR (signal-to-noise ratio) are extremely difficult to analyze and obtain the wave parameters. The selection of sample size ($M \times N$ pixels) of SAR images is the important but critical task. Computation time shows increased value for the big size datasets (Kuo *et al.*, 1999). Sea surface back scattering (Valenzuela, 1978) response senses by sensors are more dominantly affected by surface scattering phenomenon between the interactions of electromagnetic and sea surface waves.

In this paper we will introduce the simple technique to correlate SAR-derived wavelengths using Fast Fourier Transform (FFT) with the implementation of the dispersion relation to investigate wave slopes and Analysis is to be carried out over 16 sub-image areas extracted from SAR image spherical waves observed by SAR near to the coast of Chukk Island, Micronesia. Apart from the previously developed models, this method proposes the correlation between the SAR image properties with the wave hydrodynamics.

2. Experimental data and method

1) Experimental data

The ocean wave measurement is carried out by means of satellite based RADARSAT-2 SAR sensor which operates in C-band (5.4 GHz) of the electromagnetic spectrum. SAR signals are more affected due to variation in metrological conditions such as sea state, wind speed, and direction etc. Higher the wind speed rougher will be the sea surfaces; in particular, rough signatures will be appeared in SAR image due to signal smearing effect.

Fig. 1 shows the Fine quad–polarization (HH, HV, VH and VV) data acquired on November 4, 2010 at 19:40:21.60 UTC in descending orbit pass, and are mapped with ground control points (GCP) for the

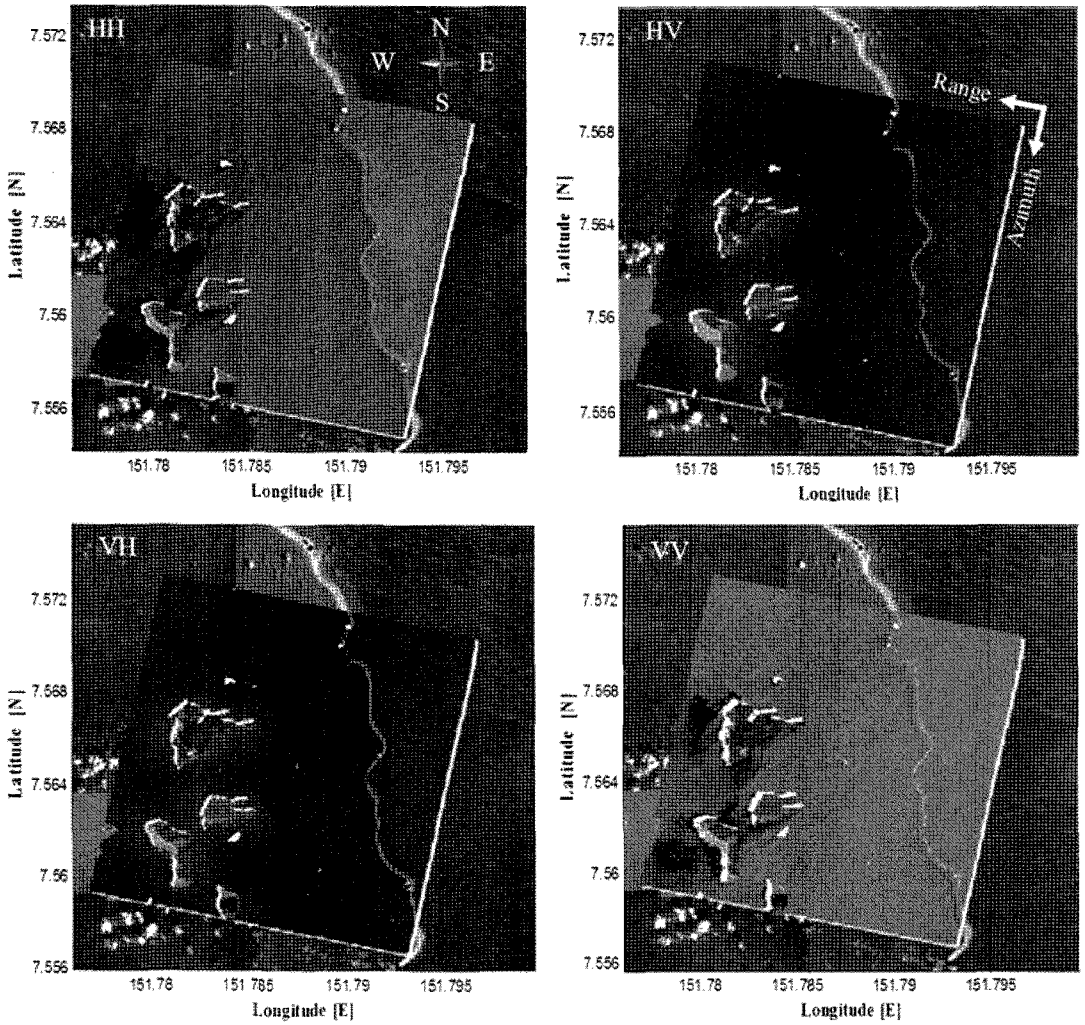

Fig. 1. RADARSAT-2 (Fine quad polarization mode) datasets acquired over the coast of Chukk, Micronesia on November 4, 2010 and geocoded with the ground control points (GCPs).

Table 1. Specification of SAR data used in this study

Satellite/ Sensor	RADARSAT-2
Mode	Fine quad polarization-Q15-HH
Date	November 4, 2010, 19:40:21.60 (UTC)
Incidence angle at scene center [deg]	35.34
Radar frequency [GHz]	5.40
Range pixel spacing [m]	4
Azimuth pixel spacing [m]	4
Orbit direction	Descending
Scene center longitude [deg]	151.92
Scene center latitude [deg]	7.41

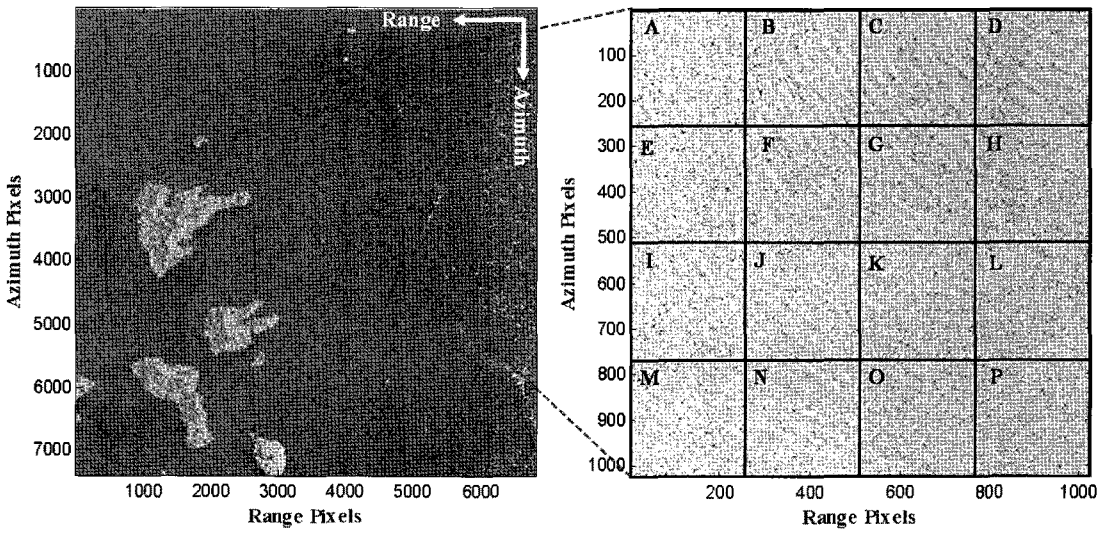

Fig. 2. SAR image for HH-polarization (left). Red square box represents the region of spherical wave signature and wave propagation signatures can easily be observed as shown in the right panel.16 different regions (A-to-P), equally spaced (256 x 256 pixels), represents the regions of interest for the estimation of wave parameters.

research site (7.74N, 151.92E), coast of Chukk Island, Micronesia and overlaid onto the optical image.

Table 1 specifies the general description of SAR image data which consists of the SAR parameters such as, its mode of an operation, radar frequency, incidence angle, azimuth and range pixel spacing etc.

Left hand side of Fig. 2 represents SAR image (HH-polarization) data used for this study, C-band SAR images are less affected under the severe metrological conditions in HH-polarization. From SAR imagery, a single image frame of size 1024×1024 pixels is to be extracted which consists of group of different sub-image areas. Red square box over an image represents the region of spherical wave pattern due to the opening of coral reefs as well as of breakwater regions.

Right hand side of the Fig. 2 represents the enlarged view of the red square frame and we divided this frame into 16 different sub-image areas (A-to-P) Each area consists of 256×256 pixels as shown in dark black square boxes. These areas are extracted to perform FFT analysis in order to estimate the

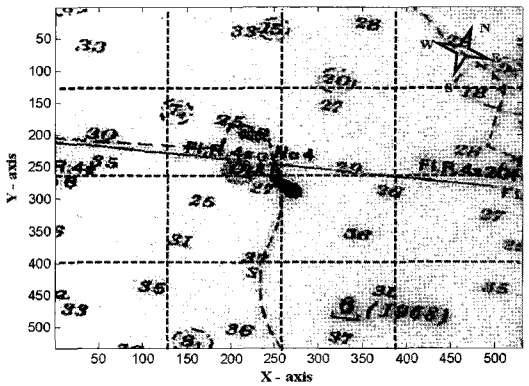

Fig. 3. Depth distribution from the navigational chart for the same region as selected in Fig. 2 (right). Each grid shows the depths for the 16 sub-images.

dominant wavelengths which will be used to estimate respective wave heights for each sub-image area. The spherical wave signatures can easily be observed in the frame and wave propagation direction can be observed from sub-image area D to M.

Depth navigational chart is illustrated in Fig. 3. Chart shows clearly the depth contour lines. It provides approximate average water depths for each sub-image area as shown with the dotted black square

Table 2. Metrological observation data for wind speed and direction on the same date as of the image acquisition.

Date(UTC)	Temperature[°C]	Wind speed[m/s]	Wind direction	Atmospheric pressure[hPa]
November 4, 2010 19:40:21	26.05	2.45	ENE	1007.50

boxes which are mapped as same as of the sub-image area represented over Fig. 2 (right). These sub-image areas belong to either intermediate or deep waters.

Table 2 tabulates the metrological data observation which represents the moderate wind condition and calms sea state. It shows the wind speed of 2.45m/s at the same date and time (November 4, 2010, 19:40:21) of an image acquisition and it shows the direction of wind from East-to-North East.

2) Method

Fig.4 represents the block diagram for estimating wave heights. First 16 sub-image areas were extracted from SAR image (HH-polarization) data as mentioned in Fig. 2 (right). FFT analysis is then carried out over all the extracted areas in order to obtain the coordinates for the peak frequency The wave numbers in range and azimuth directions can be estimated using the relationship, $k_x = \frac{2\pi P}{N\Delta x}$ and $k_y = \frac{2\pi Q}{M\Delta y}$ respectively, where M, and N are the absolute difference of pixel coordinates for peak frequencies (obtained through FFT analysis); P and Q are the number of samples and lines spacing in range and azimuth directions between peak frequencies coordinates respectively. Δx, and Δy represents pixel size resolution in range, and azimuth directions respectively (here its 4m in both range and azimuth directions). Resultant wavenumbers (k) are then estimated with the following relationship.

$$k = \sqrt{k_x + k_y} \quad (1)$$

Wave number is defined as the number of cycle traveled by a particle over unit length of distance. Further, the dominant wavelengths can be derived as,

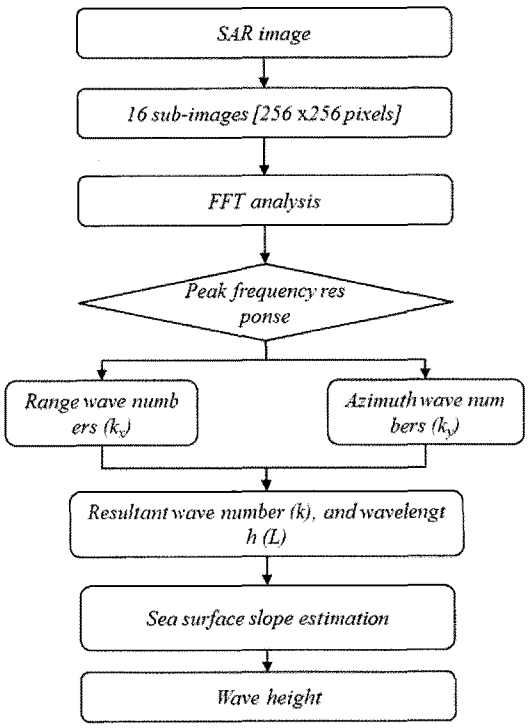

Fig. 4. Schematic block diagram for extraction of ocean wave parameters with the use of SAR.

$L = \frac{2\pi}{k}$ for each sub–image areas with the consideration of their respective resultant wavenumbers. Angular frequencies can be estimated through dispersion relation under different water wave conditions such as shallow, intermediate and deep with the use of their respective wavenumbers.

However, approximate average depths can be obtained through the Bathymetry chart for all the extracted areas. Furthermore, local sea surface slopes can be retrieved with the following relationship (Leo, 2007).

$$\alpha = \tan^{-1}\left[\frac{\omega^2 d}{g}\right] \quad (2)$$

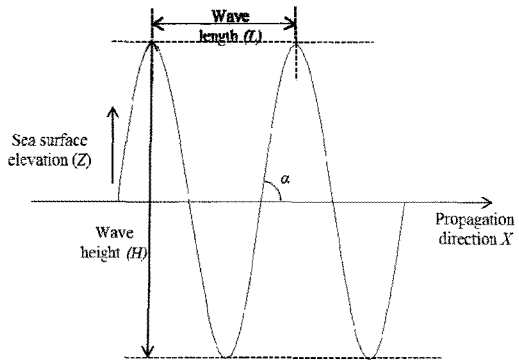

Fig. 5. Basic diagram for ocean sea surface wave as a function of sine (or cosine) wave. X-axis represents the direction of propagation and Z-axis refers to the sea surface elevation.

where ω is the angular frequency (in rad/sec) of the progressive waves, d is the water depths (in meters) below the sea surface, and g is the gravitational acceleration whose value is 9.81 m/s^2 .

Wave heights can easily be derived by the basic geometry of progressive wave as shown in Fig. 5. X and Z represent the direction of wave propagation and sea surface elevation respectively. L represents the wavelength of the sinusoidal wave and wave height (H) can easily be derived using the following relationship with usage of dominant wavelengths and sea surface slopes.

$$H = \frac{L \tan \alpha}{2\pi} \tag{3}$$

3) SAR imaging mechanism and velocity bunching concept

The generation of the spherical ocean wave phenomenon can be considered as due to the velocity bunching effects, when waves propagates radially especially in azimuth directions, hence the modulation transfer function (MTF) must be taken into account which sets up the correlation between SAR-ocean imaging mechanisms. The velocity bunching mechanism that is considered to be inherent to SAR depends on the slant range, SAR platform velocity and the orbital velocity of an ocean surface. This process is the consequence of the known effect of the shifting of an image in azimuth direction. It means that the range travelling waves shifted in the azimuth direction by an amount which is proportional to the velocity of waves.

The velocity bunching mechanism is caused by the orbital velocity of moving ocean surface waves. During the integration time of SAR line of sight to cover the particular area, the relative motion between SAR and moving surface occurs which causes a blurring effect in azimuth direction and waves spreaded azimuthally (Yang and Ouchi, 2009).

As for the range travelling waves the SAR imaging mechanism is based on tilt modulation of the water wave particles and surface scattering phenomena. Our research site is located at the place where the waves are appeared to be in spherical manner. SAR imaging mechanism is the resultant of range and azimuth images in case of spherical waves. The wave which propagates almost in the parallel to the SAR does not appear due to velocity bunching effect.

The velocity bunching formulation (Ouchi and Burridge, 1994) for an image is expressed as by the following relationship.

$$\frac{\langle I(X) \rangle}{\langle I_0 \rangle} = 1 + 2 \sum_{n=1}^{\infty} M_n \cos(nk(1 - v_0/V)X) \tag{4}$$

M_n is the nth order modulation transfer function (MTF) can be calculated as,

$$M_n = (-1)^n J_n(4k H \sin(n\omega_0 v_0 T/4)). \exp((-nk\,\Delta X/2)^2). \exp(-(nk/2)^2 (V_0/2)^2 T^2) \tag{5}$$

where J_n, I_0, v_0, V, k, X, T, ω_0, H and n are nth order Bessel function of 1st kind, mean image intensity, phase velocity, platform velocity, wavenumber, image spatial variable in azimuth direction, SAR integration time, angular frequency, wave height and Bessel's function coefficient of the waves respectively. In actual practice, there are so many discrepancies occur in validating the velocity bunching effect in SAR image

due to variation in sea state and SAR wave imaging. The variation in velocity bunching is fully dependent on the variation of Bessel's function coefficient (n) as mentioned in Eq. (5).

3. Results

Fig. 6 illustrates the classified FFT results for the sub-image areas from A-to-P respectively. The extracted wave parameters are tabulated in Table 3. Variation in wave heights depends on the obtained wavelengths through SAR and average bathymetry depths for 16 sub-image areas. The waves appeared in sub-images are in the form of high frequency sine waves propagating in the radial direction due to opening of breakwater and coral reefs. These waves are spherical in nature and are away from the SAR look direction (range propagating waves progresses radially) and Some of the sub-image areas such as P is more affected by the velocity bunching effect due to propagation component is more dominated towards azimuth direction and the peak appearance in FFT classified result is not so dominant towards the centered location of FFT result as compared to other results.

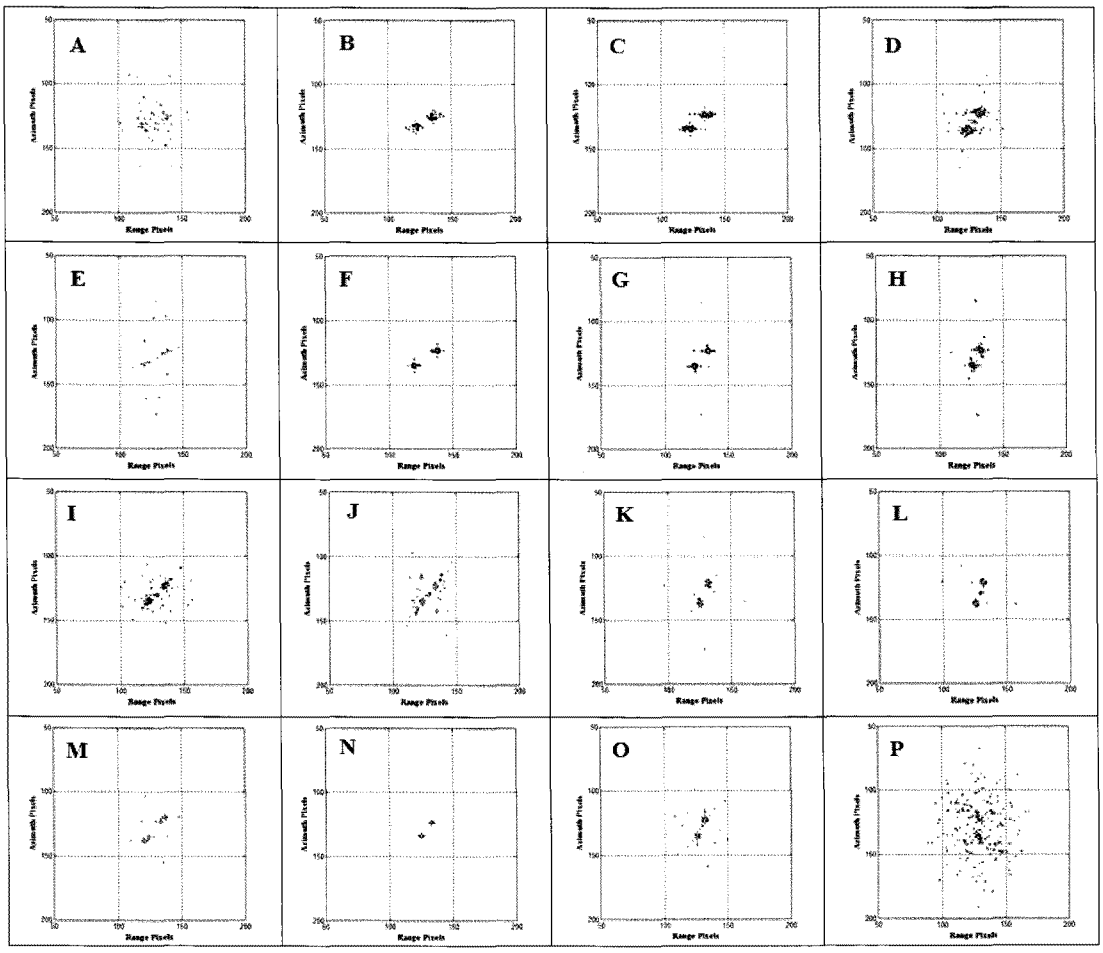

Fig. 6. Classified FFT result for sub-image area A-to-P. sub-image area P is more affected and wave parameters can not be extracted clearly.

Table 3. Result for wave parameters extracted for all 16 sub-image regions (A-to-P)

Region	Water depth, d [m]	Wavelength, L [m]	Water wave condition	Wave Slope, α [rad]	Wave height, H [m]	Direction [deg]
A	33.00	43.74	Deep	0.158	1.10	250.01
B	33.00	63.50	Deep	0.157	1.59	240.25
C	28.00	60.33	Intermediate	0.156	1.51	225.00
D	28.00	51.71	Deep	0.157	1.30	225.00
E	32.50	63.50	Deep	0.157	1.59	240.25
F	26.00	47.33	Deep	0.157	1.19	236.30
G	28.00	65.55	Intermediate	0.156	1.64	219.80
H	28.00	71.00	Intermediate	0.156	1.77	213.69
I	36.00	51.20	Deep	0.158	1.29	233.13
J	28.00	72.40	Intermediate	0.156	1.80	225.00
K	31.00	53.96	Deep	0.157	1.36	198.43
L	26.50	53.96	Intermediate	0.157	1.35	198.43
M	33.00	42.51	Deep	0.158	1.07	221.63
N	35.50	79.96	Intermediate	0.156	2.00	218.65
O	34.00	87.80	Intermediate	0.156	2.19	210.96
P	35.00	Unpredictable	Deep	NA	NA	Unpredictable

The brightness of a pixel in FFT is proportional to the amplitude of the sine waves it encodes. Sub-images B, C, F, G, H and L shows the moderate concentration of peak frequency response, while other areas shows the noisy response due to consideration of more undulation of sea surface presents in sub-image areas.

The appearance of peak of an image indicates non-linear feature of the waves. Higher frequency sine waves (indicated by bright pixels further away from center of FFT) represents the sharper edges between dark and brighter areas over an extracted sub-image. Peak appears in sub-images represents the coordinates for maximum concentration of energy and peak-to-peak distance determines the resultant wavenumbers and their respective wavelengths.

It is very necessary to estimate the water wave conditions whether the sub-image areas belong to deep, shallow or intermediate water zones. These conditions can easily be derived by use of depth to wavelength ratios. If these ratios are more than 0.5, the sub sequent area belongs to deep water otherwise in intermediate or shallow. Location of research site normally belongs to intermediate and deep water zones. Care has to be taken while the calculation of an angular frequencies with the implementation of dispersion relationship for deep as well as intermediate water wave conditions. Based on this criterion, sea surface slopes, and wave heights are estimated as per the Eqs. (2) and (3) respectively.

Fig. 7 shows the final output result which results out the direction of propagation for the different extracted sub-image areas with the representation of their respective wave heights. For example, red arrow represents wavelengths variation in between 40~50m for the areas A, F and M. White arrow belongs to the wavelengths in between 50~60m for the areas D, I, K and L. Yellow arrow represents the wavelengths variation in between 60~70m for the areas of B, C, E and G. Brown arrow indicates the wavelengths variation of 70~80m for the areas H, J and N. Black arrow represents for the wavelengths variation of 80~90m for the area O.

If we consider the area D as the origin of the

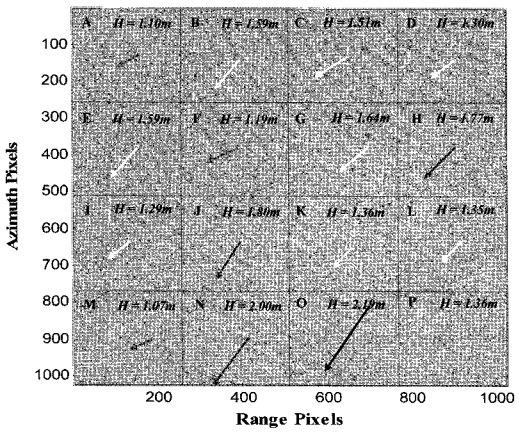

Fig. 7. Graphical representation for wave parameters as tabulated in Table 3. Arrow represents the direction with the indication of wavelengths for all 16 regions such as red arrow (L=40~50m), white arrow (L= 50~60m), yellow arrow (L=60~70m), brown arrow (L= 70~80m) and black arrow (L=80~90m). Sub-image area P represents the similar wave properties as of K with comparison of VBR and mean image intensities (please see text for detail).

spherical wave propagation and area M is the end of wave propagation over the selected image frame. We can analyze the wave heights for the areas such as D, G, J, and M is found to be 1.30m,1.64m,1.80m, and 1.07m respectively as tabulated in Table 3. Since due to shallowness and presence of an obstacle (Fig. 3) at middle of an image sub-image areas G and J are affected and hence they show the high value of wave heights. Wave height again reduces from 1.80m to 1.07m as it progresses from J to M in radial direction. This condition satisfies the spherical waves properties in ideal case, but in actual practice there should be the gradual reduction of wave heights from the point source towards the propagation direction. Also, the direction of waves in the areas F, G, K, H, F, K and O are more affected due to the effect of water shallowness and bottom topography.

Sub-image area P is more affected by velocity bunching phenomenon and it may be difficult to predict the wave parameters for this area. In order to compensate these effect, the extraction of wave Parameters for the area can easily be obtained by the velocity bunching relationship as mentioned in Eq. (4)

It can be concluded that velocity bunching ratio (VBR) decreases almost linearly with the wave height but the effect of velocity bunching increases with the wave heights because MTF increases and it Depends on the Bessel's function coefficient (n).

In order to compare the velocity bunching result for sub-image area P. The variation of VBR with wave height are as shown in Fig. 8 which represents the VBR reduces as wave height increases. VBR obtained for the sub-image area P based on MTF was found to be 0.78 at the wave height of 1.36m. In addition, the Intensity to mean image intensity ratio has also been calculated and it was found to be 0.69. Since this estimated value is less than the value obtained from through MTF and wave height of 1.36m. The respective wave height at VBR of 0.69 can be obtained from the graph as 1.75m for area P due to linear relationship. Since the variation in wave height for area P is so large as compared to area K but since here we are considering the waves progresses spherically, therefore the wave parameters for area P can be assigned same as that of K because in actual practice the VBR variation should be more closer to the estimated VBR value from MTF.

In general the spherical waves generated from the point source and decay linearly and travel with the same phase velocity along the direction of waves propagation. Since our research site is located at the place of opening of coral reefs and break waters. Waves are continuously affected by various consequences such as diffraction and interference which occurs at the different location, and time. Hence, the estimated wave height is not decaying properly along the direction of wave propagation.

Another reason for the non-uniform variation of wave parameters can be explained by means of the water depths. The obtained navigational chart is too

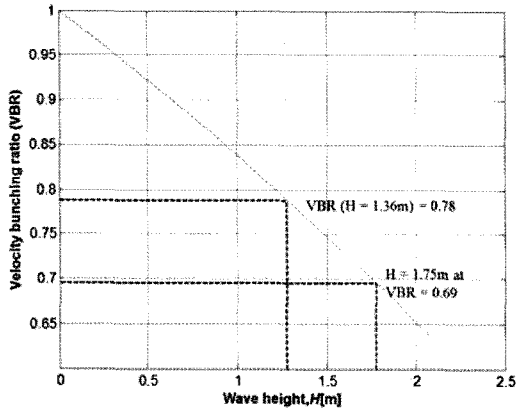

Fig. 8. Variation in velocity bunching ratio (VBR) with wave height (H), using the wave parameters obtained through the region K. VBR decays almost linearly with H and the obtained VBR at wave height of 1.36m is 0.78.

old and since the variation in water depth depends on time and their respective locations due to lack of latest depth information, it may be difficult to estimate the exact wave parameters at every particular point of interest. The variation in the waves height is as shown on Table 3 does not satisfies the decay of its amplitude in any conditions due to occurrences of wave diffraction at the research site and which shows the different signal signature patterns.

4. Summary and conclusionss

In this paper we proposed a simple technique to extract the spherical wave parameters along their propagation from a start point up to the certain distance in spherical and radial manner with the consideration of velocity bunching mechanism for azimuth traveling waves. Estimation of ocean waves by SAR is normally difficult due to dependency of radar properties such as incidence angle, look direction and imaging mechanisms, and various oceanographic phenomena such as wind speeds and sea state conditions. In this paper we proposed a simple technique to estimate the spherical wave heights for the 16 different sub-image areas (256× 256 pixels) extracted from RADARSAT -2 SAR sensor data over the coast of Chukk Island, Micronesia. FFT analysis is carried out over all the sub-image areas in order to determine the wavelengths and based on these measurements, wave slopes has been estimated for the all the sub sequent areas using dispersion relation for different water depth conditions obtained through navigational chart. Estimation of wave heights is performed using wave lengths and slopes.

Velocity bunching relationship for the sub-image area P has also been compared with the sub-image area K based on the consideration of wave properties of K. The obtained velocity bunching ratio was found to be 0.78 at the wave height of 1.36m for the sub-image P. The ratio of image intensity to mean image intensity is also being estimated for sub-image area P and it was found to be 0.69. This value is then further compared with the obtained VBR through the consideration of the VBR obtained through modulating transfer function for area P. The comparison result showed the closeness in the value of VBR for sub-image area P with both the methods. Further, it can be concluded that the wave parameters for sub-image area P is same as that of area K. Hence, the estimated wave height for sub-image area P can be assigned as 1.36m.

This work is under progress and in future, we will estimate the wave heights using polarization ratio of radar cross sections for HH- and VV-polarization data in order to estimate sea surface slope by pixel based analysis in order to test and validate the results with in-situ measurements. Also, plan is to be decided to estimate the wave parameters using the theory of radar cross section and velocity bunching effect for the spherically generated waves.

Acknowledgement

RADARSAT-2 data were provided by Canadian Space Agency (CSA), Canada. This work was supported by the Basic Research Projects (PE98641, PE98671 and PE98620) of KORDI.

References

Alpers, W., 1983. Monte carlo simulation for studying the relationship between ocean waves and SAR image spectra, *J. Geophys. Res.*, (88): 1745-1759.

Frank, M. M., and R. L. David, 1986. On the estimation of wave slope–and height–variance spectra from SAR imagery, *IEEE Trans on Geosci. and Remote Sens.*, 24 (4): 543-551.

Hasselmann, K., and S. Hasselmann, 1991. On the nonlinear mapping of an ocean wave spectrum into a synthetic aperture radar image spectrum and its inversion, *J. Geophys. Res*, 6 (96): 10713-10729.

Hasselmann, S., C. Bruuning, K. Hasselmann, and P. Heimbach, 1996. An improved algorithm for retrieval of ocean wave spectra from SAR image spectra, *J. Geophys. Res.*, 101: 16615-16629.

Kim, D.J., 2009. Wind retrieval from X-band SAR image using numerical ocean scattering model, *Korean Journal of Remote Sensing*, 25(3): 243-253.

Krogstag, H. E., 1992. A simple derivation of Hasselmann's nonlinear ocean–to–synthetic aperture radar transforms, *J. Geophys. Res.*, 77: 2421-2425.

Kuo, Y. Y., L. G. Leu, and I. L. Kao, 1996. Directional spectrum analysis and statistics obtained from ERS–1 SAR wave images, *Ocean Engineering*, 26: 1125-1144.

Leo, H., 2007. Waves in oceanic and coastal waters, Delft University of Technology and UNESCO –IHE, *Cambridge University Press.*

Ouchi, K., and C. S. Yang, 2010. Application of ALOS–PALSAR to coastal waters with examples of ship detection, and information extraction on ocean waves and underwater marine cultivation. *The 4th Joint PI Symposium of ALOS Data Nodes for ALOS Science Program*, Tokyo.

Ouchi, K., and D.A. Burridge, 1994. Resolution of a controversy surrounding the focusing mechanisms of synthetic aperture radar images of ocean waves, *IEEE Trans. Geosci. Remote Sens.*, (32): 1004-1016.

Shiroto, N., and K. Ouchi, 2010. Estimation of ocean wave height using polarization ratio of SAR data, *Proc. 32nd Symp. Remote Sens. Environ. Sci.*, 19-24.

Vachon, P.W., H. E. Krogstad, and J.S. Peterson, 1994. Airborne and spaceborne synthetic aperture radar observations of ocean waves, *Atmosphere–Ocean*, 32 (1): 83-112.

Valenzuela, G. R., 1978. Theories for the interaction of electromagnetic and ocean waves-A review, *Bound–Layer Meteor.*, 13: 61-85.

Vachon, P.W., and R. K. Raney, 1991. Resolution of ocean wave propagation direction in SAR imagery, *IEEE Trans. Geosci. Remote Sensing*, 29: 105-112.

Yang, C. S., and K. Ouchi, 2009. Wave height estimation by velocity bunching simulation using SAR data, *IEICE Tech. Rep.*, (109): 51-55.